



# Thermal stability with emission energy and Joule–Thomson expansion of regular BTZ-like black hole

Allah Ditta<sup>1,a</sup>, Xia Tiecheng<sup>1,b</sup>, G. Mustafa<sup>2,c</sup> , Muhammad Yasir<sup>1,d</sup>, Farruh Atamurotov<sup>3,4,5,6,e</sup>

<sup>1</sup> Department of Mathematics, Shanghai University, Shanghai 200444, People's Republic of China

<sup>2</sup> Department of Physics, Zhejiang Normal University, Jinhua 321004, People's Republic of China

<sup>3</sup> Inha University in Tashkent, Ziyolilar 9, 100170 Tashkent, Uzbekistan

<sup>4</sup> Akfa University, Milliy Bog' Street 264, 111221 Tashkent, Uzbekistan

<sup>5</sup> National University of Uzbekistan, 100174 Tashkent, Uzbekistan

<sup>6</sup> Tashkent State Technical University, 100095 Tashkent, Uzbekistan

Received: 22 May 2022 / Accepted: 14 August 2022 / Published online: 29 August 2022  
© The Author(s) 2022

**Abstract** We investigate the thermodynamic properties and Joule–Thomson expansion for conical or BTZ-like black holes. To analyze the thermal stability, we discuss the temperature and thermal stability relative to the horizon radius for different values of model parameters  $\beta_0$  and  $\alpha_2$ . Moreover, we analyze thermodynamical geometries like Ruppeiner, Weinhold and Hendi Panahiyah Eslam Momennia formulation and calculate respective scalar curvatures for BTZ-like black holes. Interestingly, the black holes have no singularity in some cases, i.e., completely regular. We obtain the inversion temperatures and inversion curves and investigate the similarities and differences between van der Waals and charged fluids. To discuss this expansion, we use a BTZ-like black hole. Further, we establish the position of the inversion point versus different values of mass  $\mu$ , and the parameters  $\beta_0$  and  $\alpha_2$  for such a BTZ-like black hole. The Joule–Thomson coefficient  $\mu$  at this point disappears. A crucial trait upon which we relied to inspect the sign of quantity  $\mu$  to get the cooling-heating areas. We also investigate the energy emission depending upon the frequency  $\omega$ .

## 1 Introduction

Black hole (BH) thermodynamics has been a stimulating and functional research subject with interesting results [1–7]. It is

known that thermodynamical quantities such as entropy and temperature are linked with geometrical quantities like the surface gravity and horizon area. According to semiclassical analysis, the emission of Hawking radiations makes the BHs thermally unstable. Thus, the temperature of BHs increases when their size decreases, which is a complete thermal runaway process. Several features have been disclosed about the thermodynamical properties of BHs, and one amongst them is the thermal stability of the BHs. Since thermal stability is one of the core thermodynamical properties exhibit the system's decency after a slight shift in thermodynamic parameters. A variety of techniques are available to study the phase structure of a BH near to its critical point [8]. A well-famed and formal analysis of thermal stability of BH is specific heat. The positive conduct of heat capacity physically represents that the system is thermally stable [9, 10]. The heat capacity plays a major role in studying the phase transition of BH [10–14]. There are two core types of phase transition such as heat capacity and the divergency of heat capacity.

Several authors have originated a geometrical technique for thermodynamics and phase transitions in an entirely different scenario. Hermann [15] introduced a differential manifold as an embroilment of thermodynamic phase space with a natural contact structure of subspace in an equilibrium state. In this scenario, Weinhold suggested another geometrical approach [16] by suggesting a metric of equilibrium state in thermodynamic space and the procedure of conformal mapping from Riemannian to thermodynamic space was used, which also involves the geometry of thermodynamic fluctuation. There are two attracting equilibrium states attached to the positive definite line interval in this geometry. The first amongst the two is the probability distribution of thermody-

<sup>a</sup> e-mail: [mradsahid01@gmail.com](mailto:mradsahid01@gmail.com)

<sup>b</sup> e-mail: [xiatc@shu.edu.cn](mailto:xiatc@shu.edu.cn)

<sup>c</sup> e-mails: [gmustafa3828@gmail.com](mailto:gmustafa3828@gmail.com); [gmustafa3828@zjnu.edu.cn](mailto:gmustafa3828@zjnu.edu.cn) (corresponding author)

<sup>d</sup> e-mail: [yasirciitsahiwal@gmail.com](mailto:yasirciitsahiwal@gmail.com)

<sup>e</sup> e-mail: [atamurotov@yahoo.com](mailto:atamurotov@yahoo.com)

dynamic fluctuations in Gaussian approximation. Comments about the relationships in the underlying microscopic statistical basis are put in writing in the scalar curvature of the thermodynamic quantities emerging from this geometry [17, 18]. Thus, the scalar curvature is connected with the divergency at the critical point and the correlation volume of the system.

Thermodynamical scalar curvature is visualized as the geometrical method that elaborates the macroscopic structure of the system and links it to the microscopic structure by the use of Gaussian fluctuation. In this regard, thermodynamic scalar curvature gives knowledge about the nature of microscopic interaction, which is elaborated in the research articles [19, 20]. This framework based on geometry has floated meaningful insight into divergency or phase structure and critical phenomena for BHs [21–27]. Further, thermal stability to the system is also provided by the scalar curvature [16, 28]. In classical physics, a thermodynamic system of black holes (BHs) in general relativity is analogous to the general thermodynamic system. The study is based on the four hypotheses of thermodynamics, the zero law and three other laws. Hawking was the first who proposed BH temperature [29], which means that the BHs can radiate particles near the event horizon through gravitational interactions. The thermodynamic systems of various types of black hole solutions in general relativity are very important and their properties have been widely studied [29]. The phase transition of Schwarzschild AdS BH is investigated by Hawking, and Page [30]. Later, in the extended phase space [31], the effect of the cosmological constant ( $\Lambda$ ) on the thermodynamic of BH. Regular BHs are very interesting due to the absence of central singularity. The study of thermodynamic characteristics and phase transitions of these BHs are discussed in [31, 32].

The Joule–Thomson expansion of BHs was first investigated in [33]. This subject subsequently was comprehensively studied in [34–37]. The inversion curves separating heating cooling regions in the  $T - P$  plane for isenthalpic curves with different parameters were presented. These papers show that the inversion curves  $T(P)$  for different BH systems are similar. In this paper, we would like to generalize the current research of Joule–Thomson expansion to the case of the BTZ-like BH. The paper format is as follows. In Sect. 2, we present our new class of singularity-free BH. Section 3, we comment on the thermal stability of solutions. In Sect. 4, we discuss some thermodynamical geometries like Weinhold, Ruppeiner, HPEM and GTD for BTZ-like BHs. In the next Sect. 5, we present a classical physical quantity Joule–Thomson expansion, one of the famous processes to describe the temperature change of gas from a high-pressure region to a low-pressure region through a porous plug. In Sect. 6, we discuss the energy emission phenomenon of BH. Lastly, we give some concluding remarks.

## 2 Singularity-free black hole

Seeking inspiration from the higher-dimensional counterparts present in research [38, 39], we define electromagnetic quasitopological (EMQT) structure in three dimensions by using the condition that a general Lagrangian  $\sqrt{|g|}\mathcal{L}[g^{ab}, R_{ab}, \partial_a\phi]$  reduces to a total derivative when it is evaluated on the metric [40], which is expressed as:

$$ds^2 = -f(r)dt^2 + \frac{dr^2}{f(r)} + r^2d\varphi^2, \quad \phi = p\varphi, \quad (1)$$

where  $p$  is a dimension-free arbitrary constant. We discover the given below family of densities relates to the three-dimensional EMQT structure [38]:

$$I_{EMQT} = \frac{1}{16\pi G} \int d^3x \sqrt{|g|} \left[ R + \frac{2}{L^2} - Q \right], \quad (2)$$

where

$$Q = \sum_{n=1} \alpha^n L^{2(n-1)} (\partial\phi)^{2n} - \sum_{m=0} \beta_m L^{2(m+1)} (\partial\phi)^{2m} \times \left[ (3 + 2m) R^{bc} \partial_b\phi \partial_c\phi - (\partial\phi)^2 R \right], \quad (3)$$

where  $(\partial\phi)^2 = g^{ab} \partial_a\phi \partial_b\phi$ ,  $\alpha_n$ ,  $\beta_m$  are the dimension-free constants. Notice that the terms involved in  $Q$  are linear in terms of the Ricci tensor. Thus we cannot find any evidence to ensure the existence of enhanced EMQT densities where rising powers of  $R_{ab}$  are involved. A detailed explanation is given in [41], the non-linear forms of Eq. (2) when it is being evaluated for an ansatz of the form Eq. (1). The respective expression of single and independent metric function  $f(r)$ , which once can be integrated and solved by resulting in the given below form:

$$f(r) = \left[ \frac{L^2}{r^2} - \mu - \alpha_1 p^2 \log\left(\frac{r}{L}\right) + \sum_{n=2} \frac{\alpha_1 p^{2n} L^{2(n-1)}}{2(n-1)r^{2(n-1)}} \right] \times \left[ 1 + \sum_{m=0} \frac{\beta_m p^{2(m+1)} (2m+1) L^{2(m+1)}}{r^{2(m+1)}} \right]^{-1}, \quad (4)$$

where integration constant  $\mu$  is relevant to the mass of solutions, which is expressed in the expression  $\mu = M + \beta_0 p^2 + \alpha_1 p^2 \log\left(\frac{r_0}{L}\right)$ , here  $r_0$  notions the cutoff radius. Actually, the total mass of BH is divergent as  $r_0 \rightarrow \infty$  whenever  $\alpha_1 \neq 0$ , same as in the charged BTZ solution [42]. We accentuate that Eq. (4) is the only possible static and spherically symmetric solution of Eq. (2). If one think about the more common ansatz, the equations of motion naturally put the condition  $g_{tt}g_{rr} = -1$  [41]. significantly, if all  $\alpha_n$  and  $\beta_m$  are set to zero, we get the usual static BTZ metric having mass  $\mu$ . Likewise, with only  $\alpha_1$  being active, the metric moulds in the form of charged BTZ BH [42], a fact which accompanies the electromagnetic-dual illustration of our EM-QT action. As the coupling parameters,  $\alpha_n$  and  $\beta_m$  can be turned by

will, multiparametric generalisations of the BTZ metric can be obtained.

Based on the values of parameters  $\alpha_n$  and  $\beta_m$ , Eq. (4) results in a variety of solutions. At first, the number of horizons are merely based on the positive roots of the equation

$$\frac{L^2}{r^2} - \mu - \alpha_1 p^2 \log\left(\frac{r}{L}\right) + \sum_{n=2} \frac{\alpha_1 p^{2n} L^{2(n-1)}}{2(n-1)r^{2(n-1)}} = 0, \tag{5}$$

which sequentially rely upon the values and signs of  $\alpha_n$ . Turning the effects of  $\alpha_n$  off will leads to solutions of a BH with a unified horizon  $r = L\sqrt{\mu}$  where  $\mu > 0$ , equivalent to the neutral BTZ case. Some other solutions under the effects of  $\alpha_n$  are discussed in detail in [41] which generates more than a single horizon.

At  $r = 0$ , the metric function turns to unity as

$$f(r) \stackrel{r \rightarrow 0}{=} 1, \tag{6}$$

the angular flaw existing at  $r = 0$  vanishes and the metric turns to regular [41], this is absolutely what materialises with the BTZ metric for the specific value of  $\mu = -1$ , for which it results to pure  $AdS_3$ .

The spacetime having at least one horizon describes the singularity-free BH. We are here discussing the simplest case

$$M(s, \alpha_2, \beta_0, \mu) = \frac{\alpha_2 \left( \frac{2s^{3/2}}{3\alpha_2 L^2} + \frac{2\pi^2 \beta_0^2 L^2 \sqrt{s} (\alpha_2 \mu + \alpha_2 + 2\beta_0^2)}{\alpha_2^2 (2\pi \beta_0^2 L^2 + \alpha_2 s)} - \frac{\sqrt{2\pi}^{3/2} \beta_0 L (\alpha_2 \mu + \alpha_2 + 2\beta_0^2) \tan^{-1}\left(\frac{\sqrt{\alpha_2} \sqrt{s}}{\sqrt{2\pi} \beta_0 L}\right)}{\alpha_2^{5/2}} \right)}{2\pi^{3/2}} \tag{13}$$

where  $\alpha_{1, n \geq 3} = \beta_{n \geq 1} = 0$ ,  $p^2 = 2\frac{\beta_0}{\alpha_2}$ . Then, the EMQT action takes the form of Eq. (2) where

$$\frac{Q}{L^2} = \alpha_2 (\partial\phi)^4 - \beta_0 \left[ 3R^{bc} \partial_b \phi \partial_c \phi (\partial\phi)^2 R \right] \tag{7}$$

and the solution is

$$f(r) = \frac{\frac{r^2}{L^2} - \mu + \frac{2\beta_0^2 L^2}{\alpha_2 r^2}}{1 + \frac{2\beta_0^2 L^2}{\alpha_2 r^2}}, \quad \phi = \varphi \sqrt{\frac{2\beta_0}{\alpha_2}}. \tag{8}$$

Above metric at the origin have constant Ricci scalar value  $R = \frac{3(1+\mu)\alpha_2}{L^2 \beta_0^2}$ .

We will discuss the roots to study the effects of parameters  $\alpha_2$  and  $\beta_0$  on our solutions. We can analyze other physical quantities like mass, temperature, and heat capacity. First of all, we discuss the conserved and thermodynamic features of BH. Then we calculate mass, temperature, and other thermodynamic features as an entropy function. From Eq. (8) we can obtain the mass  $\mu$  by taking  $f(r) = 0$ , as given below

$$C = \frac{T}{\frac{\partial^2 M}{\partial s^2}} = \frac{2s (2\pi \beta_0^2 L^2 + \alpha_2 s) (-2\pi^2 \beta_0^2 (\mu + 1) L^4 + 4\pi \beta_0^2 L^2 s + \alpha_2 s^2)}{-4\pi^3 \beta_0^4 (\mu + 1) L^6 + 6\pi^2 \beta_0^2 L^4 s (\alpha_2 \mu + \alpha_2 + 4\beta_0^2) + 6\pi \alpha_2 \beta_0^2 L^2 s^2 + \alpha_2^2 s^3}, \tag{15}$$

$$\mu = \frac{2\beta_0^2 L^4 + \alpha_2 r_0^4}{\alpha_2 L^2 r_0^2}, \tag{9}$$

where  $r_0$  notions the event horizon of BH. The thermal property temperature of BH can be determined by considering  $\frac{f'(r)}{4\pi}$  given below

$$T = \frac{\alpha_2 r_0 (-2\beta_0^2 (\mu + 1) L^4 + 4\beta_0^2 L^2 r_0^2 + \alpha_2 r_0^4)}{2\pi (2\beta_0^2 L^3 + \alpha_2 L r_0^2)^2} \tag{10}$$

where  $\alpha_2$  and  $\beta_0$  are coupling constants. Entropy of BH is given by

$$S = \pi r_0^2. \tag{11}$$

The total mass of the black hole can be calculated by using the first law of thermodynamics [43]

$$dM = T ds + \Phi dQ_e + \Psi dQ_m, \tag{12}$$

where  $Q_e$  and  $Q_m$  are electric and magnetic charges, respectively. Since, we are discussing an uncharged regular BH, both quantities are zero. After calculation of conserved and thermodynamical quantities, we again write the smarr-type formula in terms of entropy and coupling constants  $\alpha_2$ ,  $\beta_0$  and  $\mu$  as given:

Now, we can also find the temperature as

$$T = \frac{\alpha_2 r_0 (-2\beta_0^2 (\mu + 1) L^4 + 4\beta_0^2 L^2 r_0^2 + \alpha_2 r_0^4)}{2\pi (2\beta_0^2 L^3 + \alpha_2 L r_0^2)^2}. \tag{14}$$

The above Eq. (14) will be next used to obtain better results regarding BH solutions.

### 3 Thermal stability of solutions

The thermal stability of BH can be analysed by finding the heat capacity and divergence of roots through their positive and negative signs. Positive sign show stability and negative sign show the instability of BHs disregarding the values of the parameters used. Another useful feature of heat capacity is that it results in the relation of phase transition interpretations through its divergence [44–48]. Relation for heat capacity is given as

where

$$\frac{\partial^2 M}{\partial^2 S} = \frac{\alpha_2 (-4\pi^3 \beta_0^4 (\mu + 1) L^6 + 6\pi^2 \beta_0^2 L^4 s (\alpha_2 \mu + \alpha_2 + 4\beta_0^2) + 6\pi \alpha_2 \beta_0^2 L^2 s^2 + \alpha_2^2 s^3)}{4\pi^{3/2} L^2 \sqrt{s} (2\pi \beta_0^2 L^2 + \alpha_2 s)^3}. \quad (16)$$

Moreover, the physical and non-physical solutions of BH can be discussed by analysing the roots of temperature. The positive value of temperature ensures the physical solution of BH, while the non-physical solution is mentioned by its negative value. After recognising the thermodynamic behavior of BH, it is worth exploring the phase transition points and the bound points of heat capacity. This motive can be served by utilizing Eqs. (15) and (16) to explore the phase structure and bound points sequentially. BH system heat capacity must have a positive value to be physically stable. Heat capacity shows positive behavior by ensuring the system's stability, as shown in Fig. 1. Concerning the above discussion, one may wish to have an analysis of the roots and divergence of heat capacity. We calculate the roots of heat capacity termed as bound points [49] as given below

$$r_{0(-), BP} = -\sqrt{\frac{\sqrt{2} \sqrt{\beta_0^2 L^4 (\alpha_2 \mu + \alpha_2 + 2\beta_0^2)} - 2\beta_0^2 L^2}{\alpha_2}}, \quad (17)$$

$$r_{0(+), BP} = \sqrt{\frac{\sqrt{2} \sqrt{\beta_0^2 L^4 (\alpha_2 \mu + \alpha_2 + 2\beta_0^2)} - 2\beta_0^2 L^2}{\alpha_2}}, \quad (18)$$

and divergence points are

$$r_{0(-), DP} = -\sqrt{\frac{-2^{2/3} \alpha_2^2 \beta_0^2 L^4 (\alpha_2 \mu + \alpha_2 + 2\beta_0^2) - 2\alpha_2 \beta_0^2 L^2 \sqrt[3]{l_1} + \sqrt[3]{2} (l_1)^{2/3}}{\alpha_2^2 \sqrt[3]{l_1}}}, \quad (19)$$

$$r_{0(+), DP} = \sqrt{\frac{-2^{2/3} \alpha_2^2 \beta_0^2 L^4 (\alpha_2 \mu + \alpha_2 + 2\beta_0^2) - 2\alpha_2 \beta_0^2 L^2 \sqrt[3]{l_1} + \sqrt[3]{2} (l_1)^{2/3}}{\alpha_2^2 \sqrt[3]{l_1}}}, \quad (20)$$

where

$$l_1 = \sqrt{2} \sqrt{\alpha_2^6 \beta_0^6 L^{12} (\alpha_2 \mu + \alpha_2 + 2\beta_0^2)^2 (\alpha_2 \mu + \alpha_2 + 10\beta_0^2)} + 4\alpha_2^3 \beta_0^4 L^6 (\alpha_2 \mu + \alpha_2 + 2\beta_0^2).$$

Here, subscript B.P and D.P show the bound and divergence points, respectively. Possible roots of the heat capacity are two. For real roots they must satisfy the condition  $\alpha_2 > 0$ ,  $\beta_0 > 0$ . Figures 2 and 3 shows that positive and negative bound points and divergence points are decreasing and increasing functions of  $\alpha_2$ , i.e., as we increase  $\alpha_2$ , the BH system becomes more stable.

#### 4 Thermodynamic geometries

This section discusses the thermodynamical geometries constructed by Weinhold, Ruppeiner, Hendi Panahiyah Eslam Momennia (HPEM) and GTD [50] for BTZ-like BHs. In spite of the availability of plenty of work on the black hole thermodynamics, a full descriptive microstructure of black holes was still missing. An alternative way to Exploring the microstructure of black holes is the geometric discussion of the thermodynamic system. Here, we review the general properties of the thermodynamical geometry theories. The thermodynamic geometry connects the statistical mechanics with thermodynamics, in which a suitable metric space is decisive in the equilibrium state space of a thermodynamic system. To avoid the system's complexity, we use geometric mass  $\mu$  to discuss the geometries. Representation of Weinhold geometry in terms of mass  $\mu$  is as follows [16]

$$g_{ij}^W = \partial_i \partial_j \mu(S, \alpha_2, \beta_0). \quad (21)$$

Metric for BTZ-like BH can be expressed as

$$ds_W^2 = \mu_{SS} dS^2 + \mu_{\alpha_2 \alpha_2} d\alpha_2^2 + \mu_{\beta_0 \beta_0} d\beta_0^2 + 2\mu_{S\alpha_2} dS d\alpha_2 + 2\mu_{S\beta_0} dS d\beta_0 + 2\mu_{\alpha_2 \beta_0} d\alpha_2 d\beta_0. \quad (22)$$

Whose matrix form is given by

$$\begin{pmatrix} \mu_{SS} & \mu_{S\alpha_2} & \mu_{S\beta_0} \\ \mu_{\alpha_2 S} & \mu_{\alpha_2 \alpha_2} & 0 \\ \mu_{\beta_0 S} & 0 & \mu_{\beta_0 \beta_0} \end{pmatrix}. \quad (23)$$

curvature scalar of Weinhold metric ( $R^W$ ) from given above matrix and equations can be calculated. Weinhold curvature scalar in expression form is given below

$$R^W = -\frac{\alpha_2 s}{2\pi \beta_0^2 L^2} \quad (24)$$

It can be observed from Fig. 4 that the curvature scalar of Weinhold geometry for BTZ-like BH is singularity free, which clarifies that the Weinhold metric occupies no physical information.

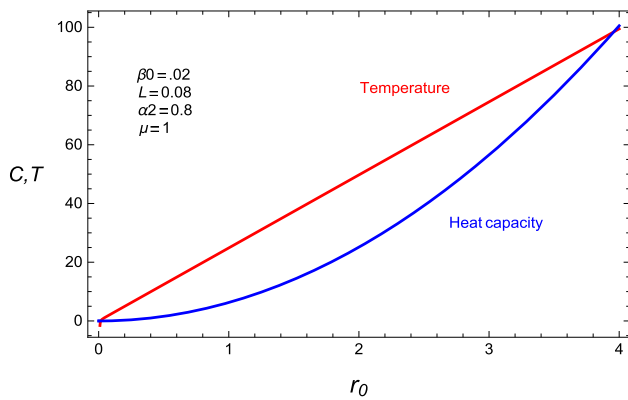


**Fig. 1** Shows the graphical behaviour of heat capacity  $C$  and temperature  $T$  for  $\beta_0 = 0.3$ ,  $L = 0.002$ ,  $\alpha_2 = 0.8$ ,  $\mu = 1$

Now we take the Ruppeiner geometry which is conformal to the Weinhold geometry. Ruppeiner metric in the thermodynamic system is elaborated as [51]

$$ds_R^2 = \frac{ds_W^2}{T}. \tag{25}$$

In expression form, Ruppeiner geometry is written as

$$R^{(Rup)} = \frac{\alpha_2^2 s^3}{2(\beta_0^2(2\pi^2\beta_0^2L^4 - \alpha_2s^2))}. \tag{26}$$

One can analyse from Fig. 5 that the curvature scalar of Ruppeiner geometry is singularity free at different values of  $\alpha_2$  and  $\beta_0$ . This can also be justified by using the HPEM formalism [52] to have an analysis of the thermodynamical properties of the BH systems.

The metric for HPEM geometry can be written as

$$ds^2 = \frac{S\mu_S}{(\frac{\partial^2\mu}{\partial\alpha_2^2} \frac{\partial^2\mu}{\partial\beta_0^2})^3} (-\mu_{SS}dS^2 + \mu_{\alpha_2\alpha_2}d\alpha_2^2 + \mu_{\beta_0\beta_0}d\beta_0^2). \tag{27}$$

The expression for HPEM geometry scalar is given by

$$R^{HPEM} = -\frac{\alpha_2^{12}s^6(2\pi^2\beta_0^2L^4 - \alpha_2s^2)}{32,768(\pi^8\beta_0^8L^{16})}. \tag{28}$$

From Fig. 6, the singularity-free behavior of the HPEM curvature scalar can be analysed to extract some meaningful information.

Relative to the microscopic explanations of interactions [53], the positive and negative curvatures inferred the repulsive and attractive interactions, respectively. It is clear from Weinhold’s curvature (see Fig. 3) that there exists a strong attractive interaction in the microstructure of regular black holes in the domain of the critical temperature of phase transitions. It is important to mention that a qualitative similarity is present between the structures of Weinhold’s geometry and Ruppeiner’s geometry, and the identical behaviour can confirm this similarity in Figs. (3 and 4). In the case of the HPEM metric, this Ricci is constructed without an additional

divergence point in the denominator of this metric. The divergence of the Ricci scalar and phase transition points of the heat capacity will harmonise. So, this formalism gives a piece of machinery that studies heat capacity. Thus, the divergence of the Ricci scalar coincides with phase transition points of heat capacity. Therefore, one can judge the type of phase transition and its behavior only by utilizing the HPEM metric.

### 5 Joule–Thomson expansion for BTZ-like black hole

A classical physical quantity, Joule–Thomson expansion is one of the famous processes to describe the temperature change of gas from a high-pressure region to a low-pressure region through a porous plug. It mainly elaborates on the process of gas expansion; this process expresses the temperature decrease as the cold effect and temperature rise as the heat effect, while enthalpy is kept constant during this expansion. This change is dependent upon the Joule Thomson coefficient, which is given by:

$$U_{JT} = \left(\frac{\partial T}{\partial P}\right)_H = \frac{1}{C_p} \left[ T \left(\frac{\partial V}{\partial T}\right)_p - V \right], \tag{29}$$

where heat capacity at constant pressure is given by

$$c_p = \left(\frac{\partial S}{\partial T}\right)_p. \tag{30}$$

The entropy obtained at the event horizon by the area law is given by

$$S = \pi r_0^2, \tag{31}$$

and

$$P = -\frac{\Lambda}{8\pi} = \frac{3}{8\pi L^2}. \tag{32}$$

The first law of the black hole is given by

$$d\mu = TdS + VdP + \varphi d\beta_0,$$

and all the thermodynamic variables defined above can be obtained as follows

$$T = \left(\frac{\partial\mu}{\partial S}\right)_{P,\beta_0}, \quad V = \left(\frac{\partial\mu}{\partial P}\right)_{S,\beta_0}, \quad \varphi = \left(\frac{\partial\mu}{\partial\beta_0}\right)_{S,P}. \tag{33}$$

Using  $f(r) = 0$ , the mass of BH can be written as

$$\mu = \frac{3\beta_0^2}{4\pi\alpha_2 Pr^2} + \frac{8}{3}\pi Pr^2. \tag{34}$$

$$T = \frac{2\alpha_2 Pr_0(32\pi^2\alpha_2 P^2 r_0^4 + 3\beta_0^2(16\pi Pr_0^2 - 3(\mu + 1)))}{3(3\beta_0^2 + 4\pi\alpha_2 Pr_0^2)^2}. \tag{35}$$

The volume of BH as

$$V = \frac{8\pi r_0^2}{3} - \frac{3\beta_0^2}{4\pi\alpha P^2 r_0^2}. \tag{36}$$

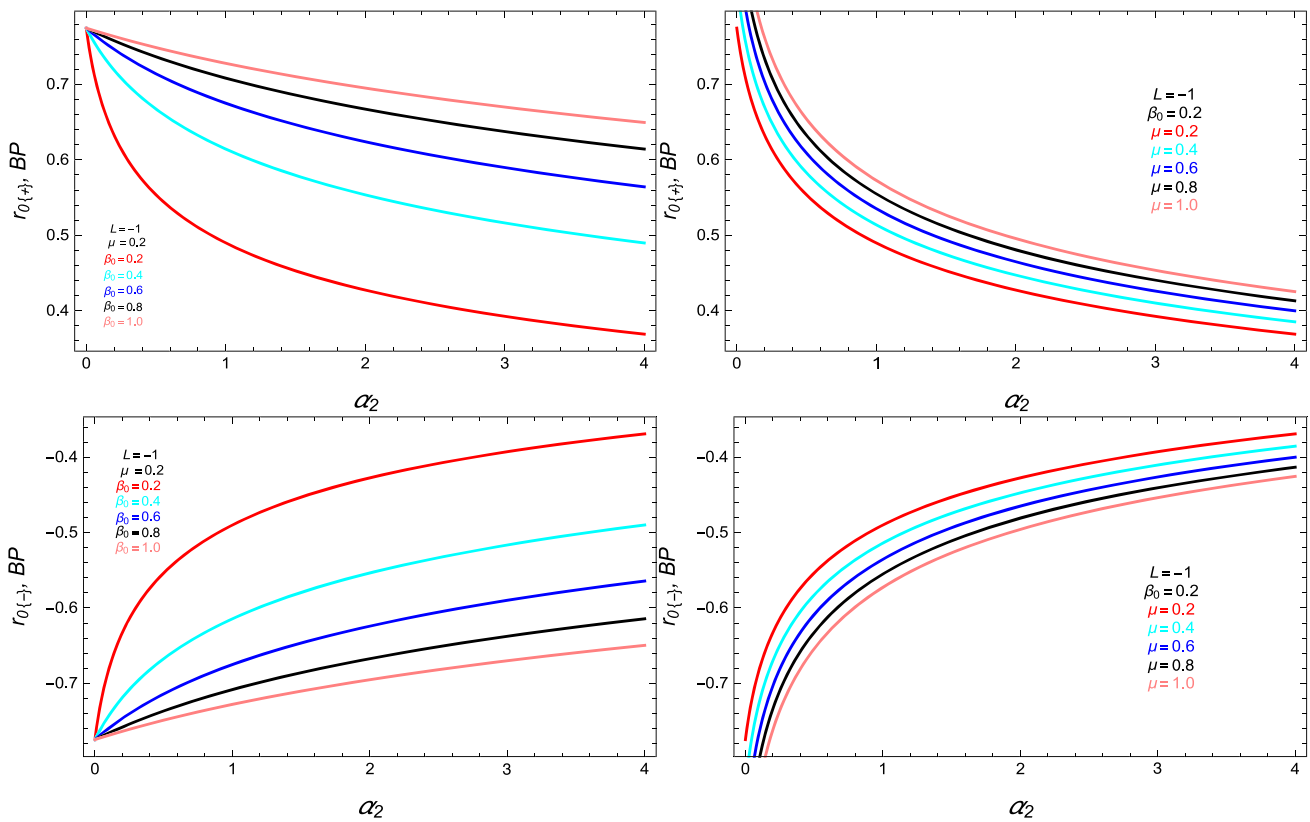


**Fig. 2** Positive and negative bound points (BP)  $r_{0(+)}$ , and  $r_{0(-)}$  (up and down) plots along  $\alpha_2$  for by fixing  $L = -1$ ,  $\mu = 0.2$  for different values of  $\beta_0$  {left panel} and positive and negative bound points (BP)  $r_{0(+)}$ , and  $r_{0(-)}$  (up and down) plots along  $\alpha_2$  for by fixing  $L = -1$ ,  $\beta_0 = 0.2$  for different values of  $\mu$  {right panel}

Potential of BH as

$$\varphi = \frac{3\beta_0}{2\pi\alpha Pr_0^2}. \tag{37}$$

The pressure should be

$$P = \frac{3 \left( \sqrt{\alpha_2^2 \mu^2 r_0^4 - 8\alpha_2 \beta_0^2 r_0^4} + \alpha_2 \mu r_0^2 \right)}{16\pi\alpha_2 r_0^4}. \tag{38}$$

$$\mu_{JT} = \frac{64\pi^2\alpha_2 Pr_0^4}{24\pi^2\alpha_2 Pr_0^3 + 18\pi\beta_0^2 r_0} - \frac{24\pi^2\alpha r_0^3 (32\pi^2\alpha_2 P^2 r_0^4 - 9\beta_0^2)}{(24\pi^2\alpha_2 Pr_0^3 + 18\pi\beta_0^2 r_0)^2}. \tag{39}$$

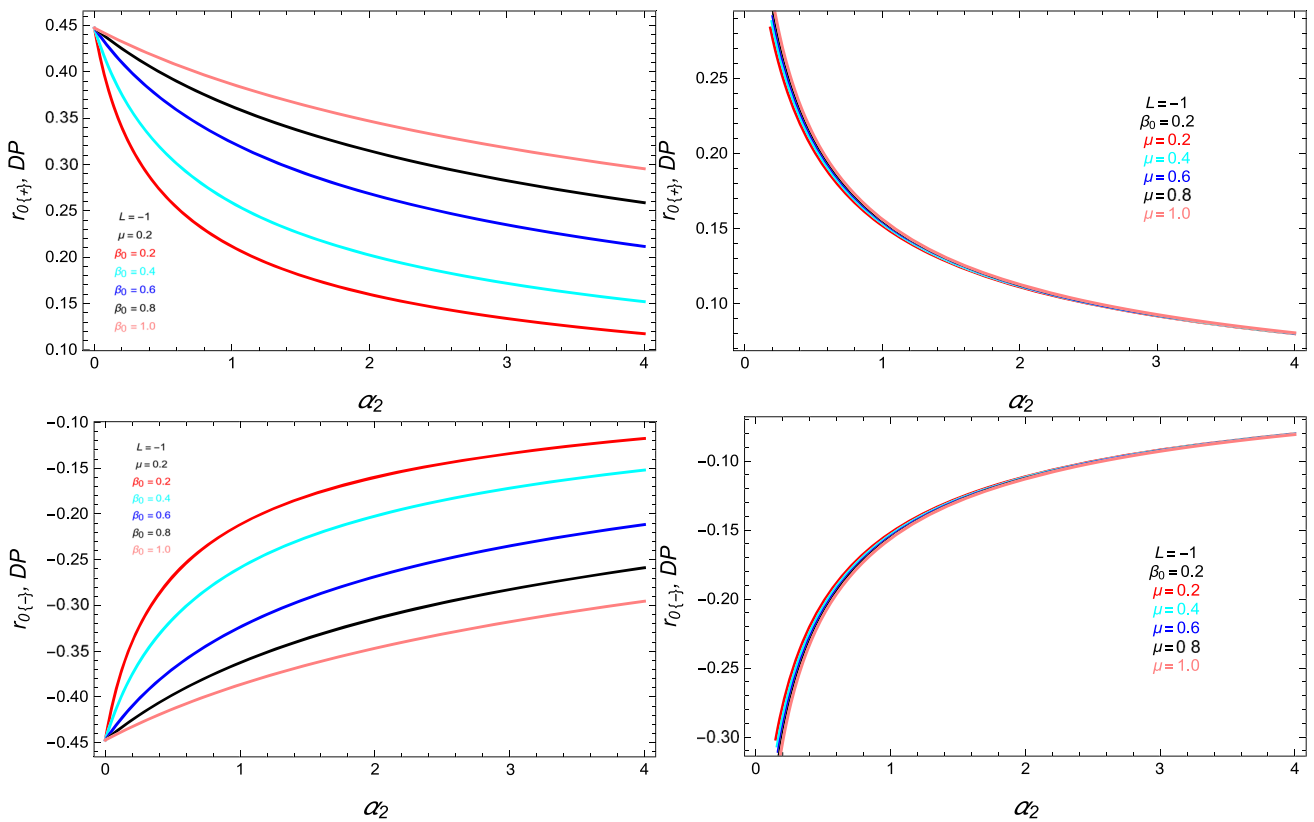
From the definition of Joule- Thomson expansion, we can extract the inversion temperature as

$$T_i = \frac{(32\pi^2\alpha_2 P^2 r_0^4 - 9\beta_0^2) (27\beta_0^4 + 128\pi^3\alpha_2^3 P^3 r_0^6 + 36\pi\alpha_2 \beta_0^2 Pr_0^2 (8\pi Pr_0^2 + 3))}{6 (32\pi^3\alpha_2 P^3 r_0^4 + 9\pi\beta_0^2 P) (4\pi\alpha_2 Pr_0^3 + 3\beta_0^2 r_0)^2}. \tag{40}$$

The cooling-heating regions can be expressed by the sign of Eq. (38). Because the pressure always decreases during expansion so that temperature increase or decrease affects the sign of coefficient  $\mu$ , if the change of temperature is positive, it leads to the cooling region; when the temperature is negative, it leads to the heating region.

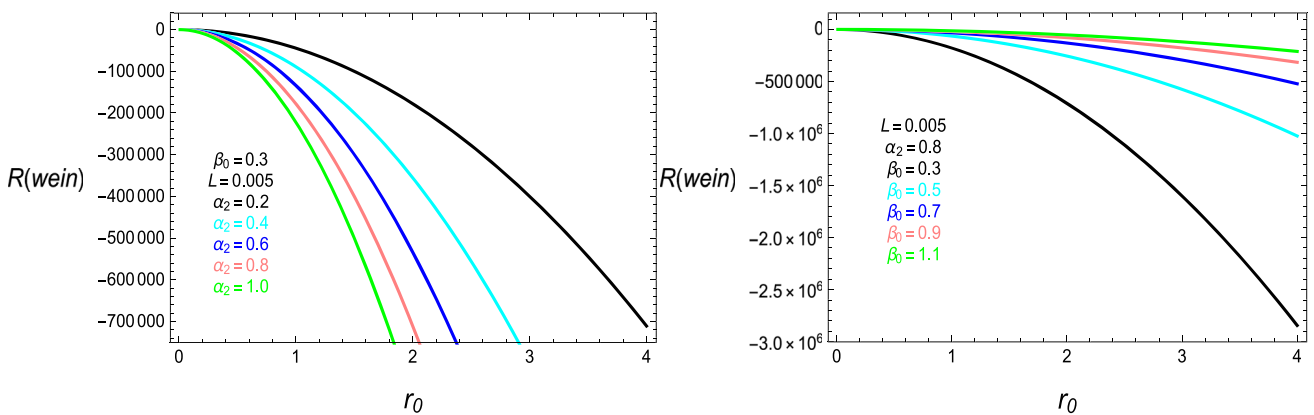
From the above Joule–Thomson expansion equation coefficient obtained is as given:

Figure 7 shows the temperature behaviour with increasing values of  $\beta_0$  and fixed pressure for regular BTZ-like BH. The temperature decreases under the region  $r_0 \leq 0.4$ , leading to the unstable region, but greater than 0.4 represents the thermodynamically stable region. Figure 8 demonstrates that regular BTZ-like BH is always thermodynamically (mass) stable with positive  $\alpha_2 = 2$  and  $\alpha_2 = 4$ . In addition, for increasing pressure values  $\beta_0$  and  $r_0$ , the local maximum of  $\mu$  decreases. Further, the  $\mu$  converges when  $r_0$  shrinks to zero for regular BTZ-like BH. Figure 9 represents the inversion temperature



**Fig. 3** Positive and negative divergence points (DP)  $r_{0(+)}$ , and  $r_{0(-)}$  (up and down) plots along  $\alpha_2$  for by fixing  $L = -1$ ,  $\mu = 0.2$  for different values of  $\beta_0$  {left panel} and positive and negative

points (DP)  $r_{0(+)}$ , and  $r_{0(-)}$  (up and down) plots along  $\alpha_2$  for by fixing  $L = -1$ ,  $\beta_0 = 0.2$  for different values of  $\mu$  {right panel}



**Fig. 4** Wein Hold geometry  $R(wein)$  plots, for  $\beta_0 = 0.3$ ,  $L = 0.005$ ,  $\alpha_2 = (0.2, 0.4, 0.6, 0.8, 1.0)$  {left} and  $\alpha_2 = 0.8$ ,  $L = 0.005$ ,  $\beta_0 = (0.3, 0.5, 0.7, 0.9, 1.1)$  {right}

$T_i$  for increasing values of parameter  $\alpha_2$  and  $\beta_0$ . We can see that from the figures, the inversion curves are not closed, with the lowest inversion curve comparable with Van der Waals fluids. The inversion temperature is inversely related to the values of parameter  $\alpha_2$  and  $\beta_0$  of regular BTZ-like BH, and it is habituated to separate the cooling and heating regimes. In all the three trajectories, the position of inversion point  $T_i$  shifts to the higher values with an increase in the parameter

$\beta_0$ . The Joule–Thomson coefficient  $\mu_{JT}$  in terms of horizon  $r_0$  is shown in Fig. 10. We fix  $\alpha_2 = 0.1$  and  $\alpha_2 = 0.2$ , the parameter  $\beta_0$  as 0.02, 0.04, 0.06 in order. Both divergence points are less than zero of horizon radius  $r_0$ . By comparing the above figures, we can demonstrate that the divergence point of the Joule–Thomson coefficient is reconcilable with the zero point of Hawking temperature. The divergence point

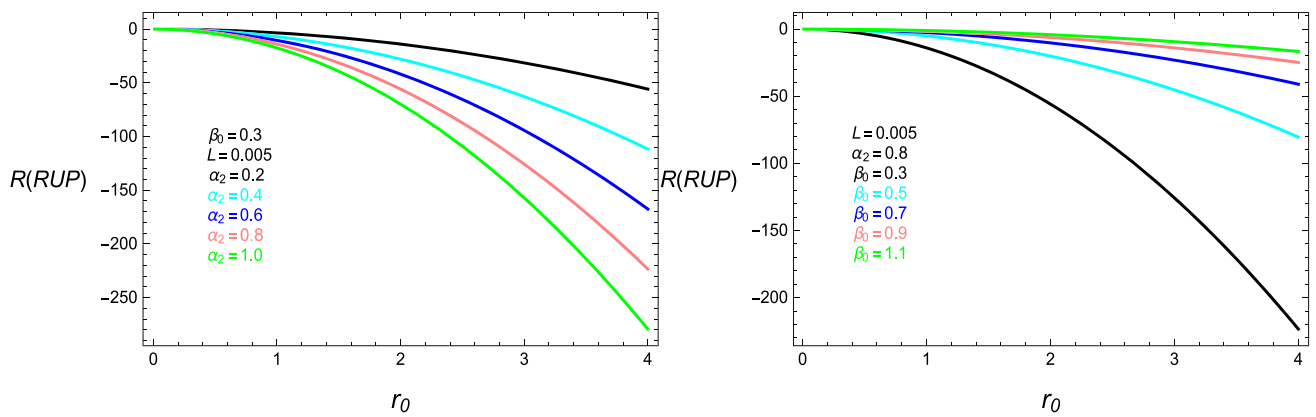


**Fig. 5** Shows Rupenior geometry  $R(RUP)$  by taking  $\beta_0 = 0.3$ ,  $L = 0.005$ ,  $\alpha_2 = (0.2, 0.4, 0.6, 0.8, 1.0)$  {left} and  $\alpha_2 = 0.8$ ,  $L = 0.005$ ,  $\beta_0 = (0.3, 0.5, 0.7, 0.9, 1.1)$  {right}

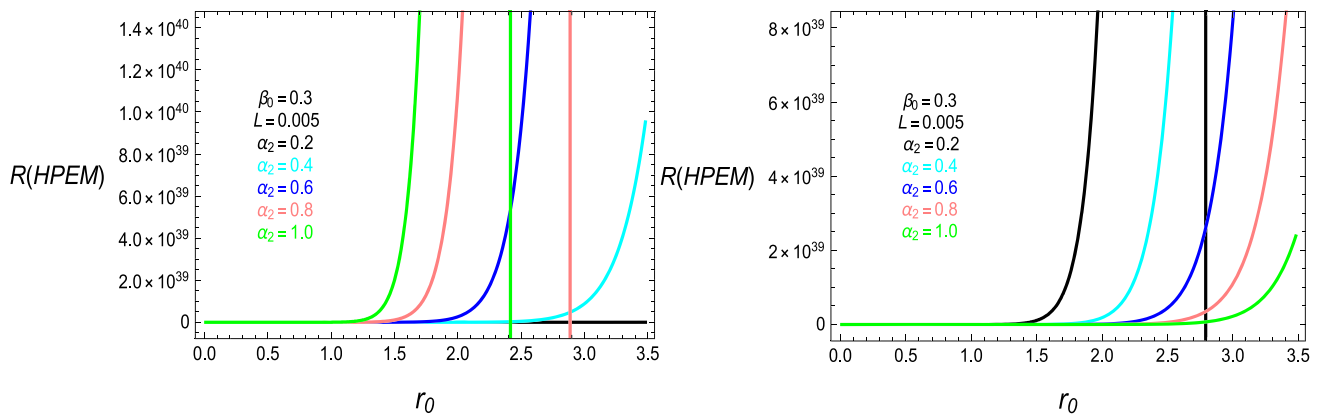


**Fig. 6** Portray the graphical behavior of  $HEPM$  geometry by choosing  $\beta_0 = 0.3$ ,  $L = 0.005$ ,  $\alpha_2 = (0.2, 0.4, 0.6, 0.8, 1.0)$  {left} and  $\alpha_2 = 0.8$ ,  $L = 0.005$ ,  $\beta_0 = (0.3, 0.5, 0.7, 0.9, 1.1)$  {right}

contains the Hawking temperature information and corresponds to the extremal black hole.

Figure 11 represents the isenthalpic curves with constant mass (enthalpy) for various values of parameter  $\beta_0$  in the  $T - P$  plane. The inversion curves and isenthalpic curves describe the cooling and heating regions. The inversion curves separate and distinguishes the plane of isenthalpic curves into two regions. The left side region of the inversion curve denotes the warm phase, whereas the temperature increases and the right-side portion of the curve represent the cooling process. In detail, one can also check the sign of the slope of isenthalpic curves in the cooling or heating phases. The slope should be positive in the cooling region, and if it turns negative, it will represent the heating region. Inversion curves are a barrier between the heating and cooling regimes.

### 6 Emission energy

It is known that quantum fluctuations in the interior of the BHs cause the formation and eradication of an excessive

number of particles very close to the horizon. The particles having positive energy get out from the BH via tunneling in the core region where Hawking radiation occurs, which becomes the main reason for the BH evaporation in some specific period. In this section, we intend to discuss the energy emission rate associated with it. For a distant observer, the cross-section of high-energy reception approaches the BH shadow. The energy reception cross-section of the BH at very high energy oscillates to the constant and limiting value  $\sigma_{lim}$ . It addresses that this constant and limiting value is associated with the radius of BH as [54–56]:

$$\sigma_{lim} \approx \pi R_0^2, \tag{41}$$

where,  $R_0$  notions the BH horizon radius. Thus the expression for energy emission rate of BH is [54–56]:

$$\frac{d^2\varepsilon}{d\omega dt} = \frac{2\pi^2\sigma_{lim}}{\exp\frac{\omega}{T} - 1} \omega^3, \tag{42}$$

where, the temperature  $T$  is given in Eq. (14). Equation (42) becomes after replacement of horizon radius  $r_0$ , temperature  $T$  and cross section  $\sigma_{lim}$  as:



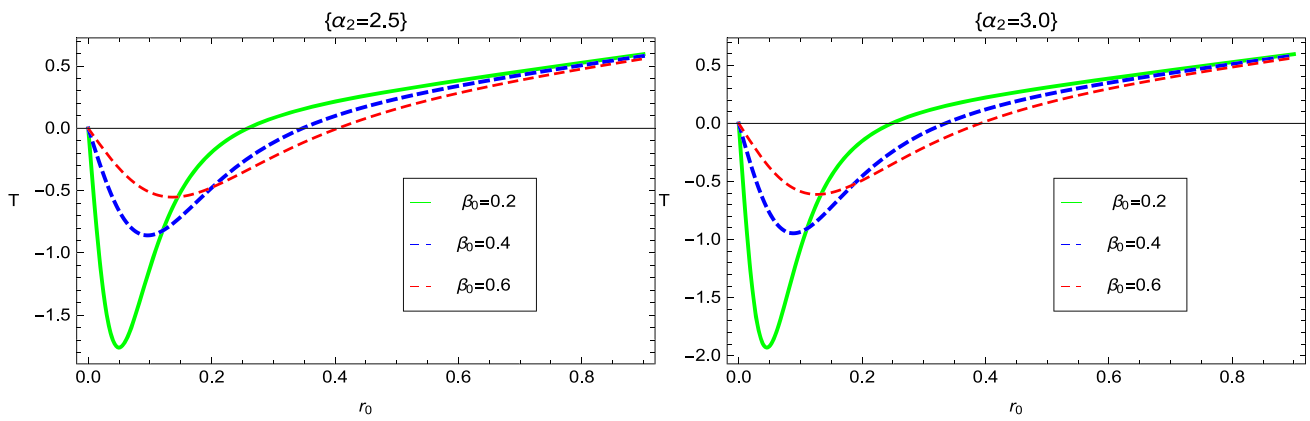


**Fig. 7** Temperature  $T$  plot with fixed value of  $\alpha_2 = 2.5$  and  $\beta_0 = (0.2, 0.4, 0.6)$  {left} and  $\alpha_2 = 3.0$  and  $\beta_0 = (0.2, 0.4, 0.6)$  {right}

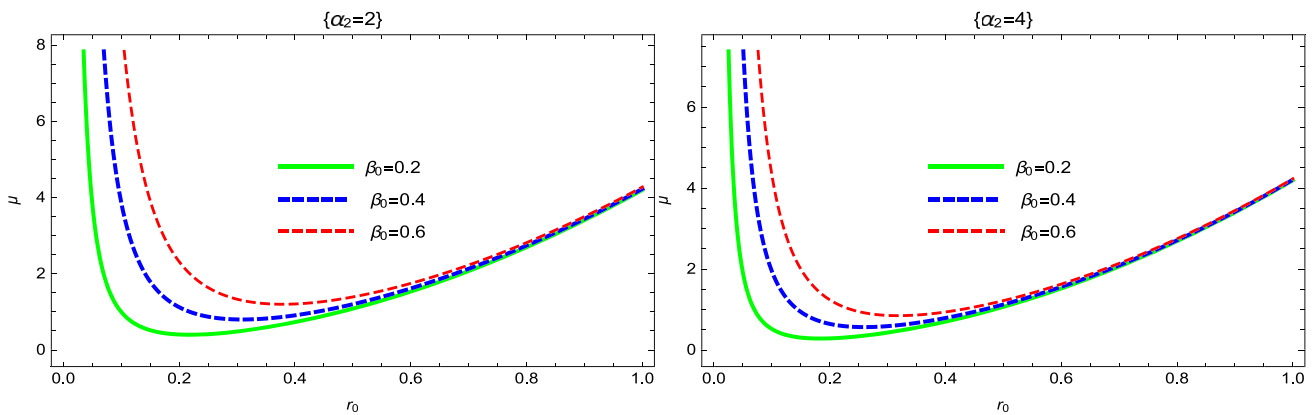


**Fig. 8** Plot of Mass with fixed value of  $\alpha_2 = 2.0$  and  $\beta_0 = (0.2, 0.4, 0.6)$  {left} and  $\alpha_2 = 4.0$  and  $\beta_0 = (0.2, 0.4, 0.6)$  {right}

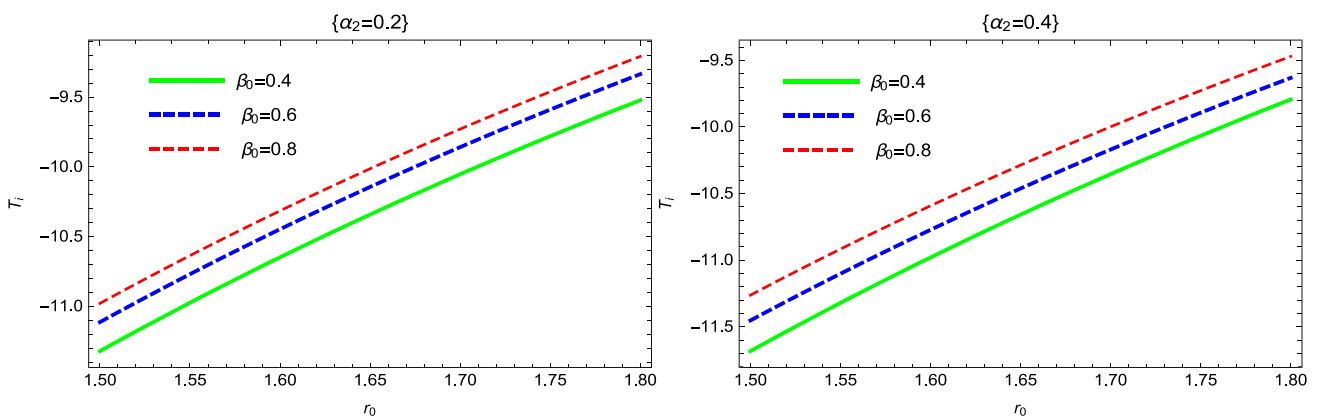


**Fig. 9** Plot of inversion temperature with fixed of  $\alpha_2 = 2$  and  $\beta_0 = (0.4, 0.6, 0.8)$  {left} and  $\alpha_2 = 4.0$  and  $\beta_0 = (0.4, 0.6, 0.8)$  {right}

$$\frac{d^2\varepsilon}{d\omega dt} = \frac{\sqrt{2}\pi^3\omega^3 \sqrt{L^2 \left( \frac{\sqrt{\alpha_2\mu^2 - 8\beta_0^2}}{\sqrt{\alpha_2}} + \mu \right)}}{\exp \left( \frac{\sqrt{2}\pi\omega \left( \sqrt{\alpha_2}\sqrt{\alpha_2\mu^2 - 8\beta_0^2} + \alpha_2\mu + 4\beta_0^2 \right) \sqrt{L^2 \left( \frac{\sqrt{\alpha_2\mu^2 - 8\beta_0^2}}{\sqrt{\alpha_2}} + \mu \right)}}{\sqrt{\alpha_2}\mu\sqrt{\alpha_2\mu^2 - 8\beta_0^2} + \alpha_2\mu^2 - 8\beta_0^2} \right)} - 1, \tag{43}$$

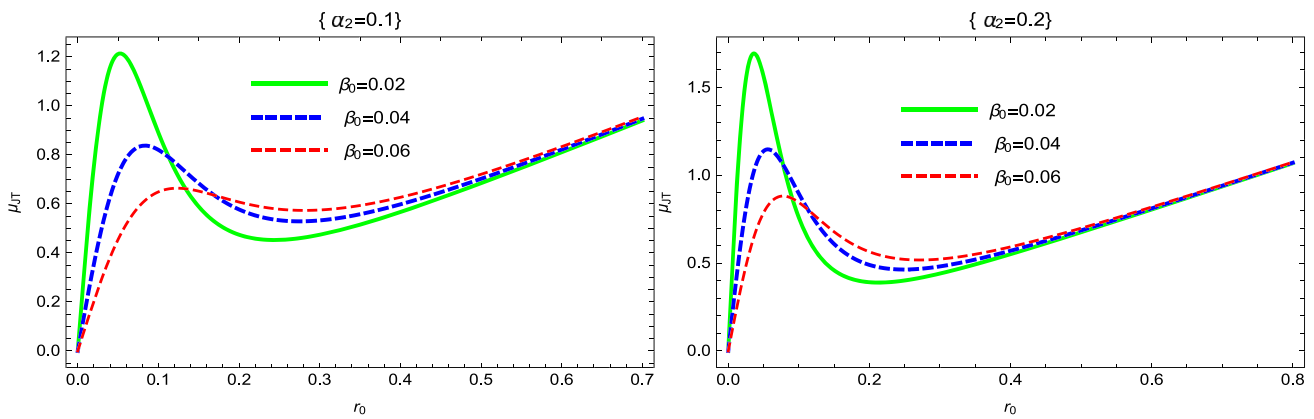


**Fig. 10** Plot of Joule–Thomson Coefficient with fixed value of  $\alpha_2 = 0.1$  and  $\beta_0 = (0.02, 0.04, 0.06)$  {left} and  $\alpha_2 = 0.2$  and  $\beta_0 = (0.02, 0.04, 0.06)$  {right}

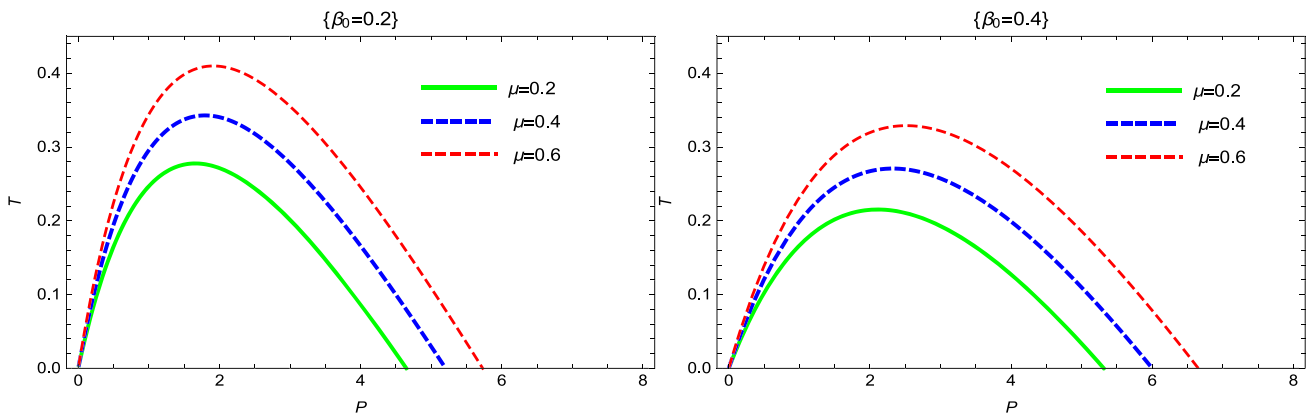


**Fig. 11** Plot of isenthalpic curves with fixed value of  $\beta_0 = 0.2$  and  $\mu = (0.2, 0.4, 0.6)$  {left} and  $\beta_0 = 0.4$  and  $\mu = (0.2, 0.4, 0.6)$  {right}

where,  $\alpha_2, \beta_0, L$  are constant parameters and  $\mu$  is the mass of BH. Energy emission variations for different values of  $\alpha_2, \beta_0$  are graphed in Fig. 12. In Fig. 12 for the purpose of simplicity  $\frac{d^2\varepsilon}{d\omega d\tau} = \varepsilon_{\omega\tau}$ . It can be seen that energy emission rate vary by the varying the parameters  $\alpha_2$  and  $\beta_0$ .

### 7 Conclusion

In this article, we have evaluated the conserved and thermodynamic quantities of the BTZ-Like BH and calculated the Smarr-type formalism for the mass as a function of the extensive variables. After that, we presented a comprehensive analysis of the thermodynamics and stability of BH. We discussed the thermal stability of the BTZ-Like BH and found the possible number of bounds relying upon the coupling parameters  $\alpha_2$  and  $\beta_0$ . From Fig. 1, it is clear that the positive behavior of heat capacity shows the thermal stability of the BH. Figures 2 and 3 depicts the positive and negative behavior for positive real values of coupling parameters (i.e.,  $\alpha_2 > 0$  and  $\beta_0 > 0$ ). Moreover, we have established the geometrical composition of BTZ-Like BH by using the

Weinhold, Ruppeiner, and HPEM dogmatism. Figures 4 and 5 show the singularity-free behavior of Weinhold and Ruppeiner geometry which have no physical interpretations; they only show the attractive interaction due to negative behaviour. Whereas Fig. 6 has positive behavior and is free of singularity, some meaningful information can be extracted as mentioned in section-IV.

It is important to discuss that our study mainly involves parameters  $L, \beta_0, \alpha_2,$  and  $\mu$ , so their negative and positive signs are of much importance. It is note-able that the negative value of  $\alpha$  may generate a complex value, like in divergence and bound points, so we always take  $\alpha > 0$ . Since  $\beta_0$  and  $L$  are squared quantities, their negative and positive values have no impact on the behaviour of solutions. Also,  $\mu$  is the geometric mass of the regular black hole, so it cannot be negative; thus,  $\mu > 0$ .

This paper also discusses the Joule–Thomson expansion for BTZ-like BH, where the cosmological constant is written with the pressure. Since the BH mass is clarified as enthalpy, it is defined as the mass that does not change during the Joule–Thomson expansion. The Joule–Thomson coefficient  $\mu_{JT}$  versus the horizon  $r_0$  is shown in Fig. 10, which shows

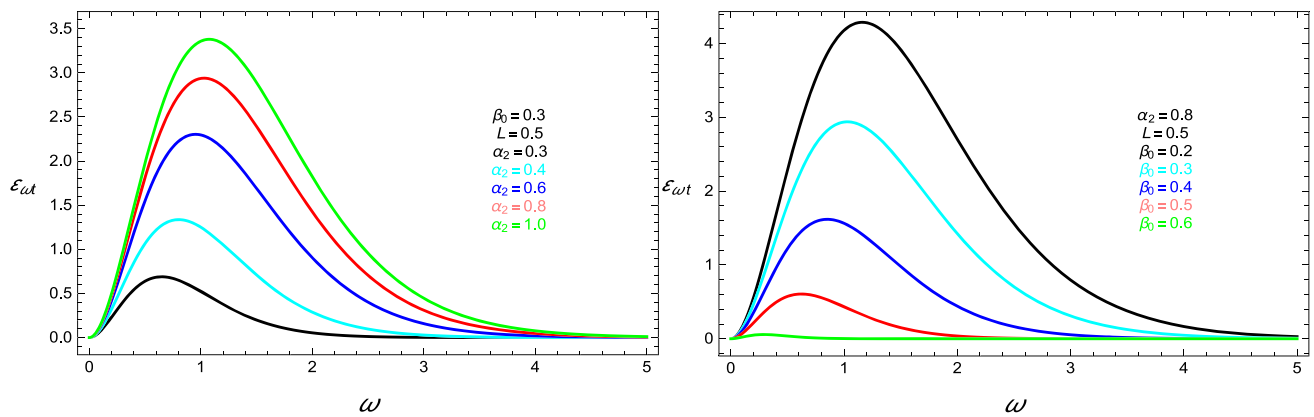


**Fig. 12** Plots for the rate of energy emission varying with the frequency with fixed value of  $\beta_0 = 0.3$  and  $\alpha_2 = (0.3, 0.4, 0.6, 0.8, 1.0)$  {left} and  $\alpha_2 = 0.8$  and  $\beta_0 = (0.2, 0.3, 0.4, 0.5, 0.6)$  {right}

that both of the divergence points are zero and less than the horizon radius  $r_0$ . By comparing the above figures, we can demonstrate that the divergence point of the Joule–Thomson coefficient is reconcilable with the zero point of Hawking temperature. The divergence point contains the Hawking temperature information and corresponds to the extremal black hole. Since the BH mass is interpreted as enthalpy, an isenthalpic technique can be applied to obtain the temperature change during the Joule–Thomson expansion. And we calculated the inversion curves in the  $T - P$  (Fig. 11) plane and the corresponding isenthalpic curves. We have investigated the inversion curves which distinguish the cooling and heating regions for different values of  $\alpha_2$  and  $\beta_0$ . Finally, the energy emission rate, dependent on the frequency  $\omega$ , is elaborated in Fig. 12. It is noted that the energy emission rate varies by the variation in the parameters  $\alpha_2$  and  $\beta_0$ .

**Acknowledgements** The paper was funded by the National Natural Science Foundation of China 11975145. G. Mustafa is very thankful to Prof. Dr. Xianlong Gao from the Department of Physics, Zhejiang Normal University, for his kind support and help during this research. Further, G. Mustafa acknowledges the Grant no. ZC304022919 to support his Postdoctoral Fellowship at Zhejiang Normal University. F.A. acknowledges the support of INHA University in Tashkent and research work has been supported by the Visitor Research Fellowship at Zhejiang Normal University. This research is partly supported by Research Grant FZ-20200929344; F-FA-2021-510 of the Uzbekistan Ministry for Innovative Development.

**Data Availability Statement** This manuscript has no associated data, or the data will not be deposited. (There are no observational data related to this article. The necessary calculations and graphic discussion can be made available on request.)

**Open Access** This article is licensed under a Creative Commons Attribution 4.0 International License, which permits use, sharing, adaptation, distribution and reproduction in any medium or format, as long as you give appropriate credit to the original author(s) and the source, provide a link to the Creative Commons licence, and indicate if changes were made. The images or other third party material in this article are included in the article's Creative Commons licence, unless indicated otherwise in a credit line to the material. If material is not

included in the article's Creative Commons licence and your intended use is not permitted by statutory regulation or exceeds the permitted use, you will need to obtain permission directly from the copyright holder. To view a copy of this licence, visit <http://creativecommons.org/licenses/by/4.0/>.

Funded by SCOAP<sup>3</sup>. SCOAP<sup>3</sup> supports the goals of the International Year of Basic Sciences for Sustainable Development.

## References

1. J.D. Bekenstein, Black holes and entropy. *Phys. Rev. D* **7**, 2333–2346 (1973)
2. J.D. Bekenstein, Generalized second law of thermodynamics in black-hole physics. *Phys. Rev. D* **9**, 3292–3300 (1974)
3. S.W. Hawking, Particle creation by black holes. *Commun. Math. Phys.* **43**, 199 (1975)
4. S.W. Hawking, Black holes and thermodynamics. *Phys. Rev. D* **13**, 191 (1976)
5. S.W. Hawking, D.N. Page, Thermodynamics of black holes in anti-de sitter space. *Commun. Math. Phys.* **87**, 577 (1983)
6. J.M. Bardeen, B. Carter, S.W. Hawking, The four laws of black hole mechanics. *Commun. Math. Phys.* **31**, 161 (1973)
7. G.W. Gibbons, S.W. Hawking, Action integrals and partition functions in quantum gravity. *Phys. Rev. D* **15**, 2752 (1977)
8. D. Kubiznak, R.B. Mann, P–V criticality of charged AdS black holes. *JHEP* **033**, 1207 (2012)
9. T. Padmanabhan, *Class. Quantum Gravity* **21**, 4485 (2004)
10. Y.S. Myung, *Phys. Rev. D* **77**, 104007 (2008)
11. P.C.W. Davies, Thermodynamic phase transitions of Kerr–Newman black holes in de sitter space. *Class. Quantum Gravity* **6**, 1909 (1989)
12. S. Sumati, S. Kristin, M.W. Donald, Phase transitions for flat anti-de sitter black holes. *Phys. Rev. Lett.* **86**, 5231 (2001)
13. Z. De-Cheng, Z.J. Shao, W. Bin, Critical behavior of Born–Infeld AdS black holes in the extended phase space thermodynamics. *Phys. Rev. D* **89**, 044002 (2014)
14. A. Sahay, T. Sarkar, G. Sengupta, Thermodynamic geometry and phase transitions in Kerr–Newman–AdS black holes. *JHEP* **1004**, 118 (2010)
15. R. Hermann, *Geometry, Physics and Systems* (Marcel Dekker, New York, 1973)
16. F. Weinhold, Metric geometry of equilibrium thermodynamics. *J. Chem. Phys.* **63**, 2479 (1975)

17. P. Chaturvedi, A. Das, G. Sengupta, Thermodynamic geometry and phase transitions of dyonic charged AdS black holes. *Eur. Phys. J. C* **77**, 110 (2017)
18. F. Capela, G. Nardini, *Phys. Rev. D* **86**, 024030 (2012)
19. A. Sahay, T. Sarkar, G. Sengupta, On the thermodynamic geometry and critical phenomena of AdS black holes. *J. High Energy Phys.* **07**, 1 (2010)
20. B. Mirza, H. Mohammadzadeh, Ruppeiner geometry of anyon gas. *Phys. Rev. E* **78**, 021127 (2008)
21. S. Gunasekaran, R.B. Mann, D. Kubiznak, Extended phase space thermodynamics for charged and rotating black holes and Born–Infeld vacuum polarization. *J. High Energy Phys.* **11**, 010 (2012)
22. A. Rajagopal, D. Kubiznak, R.B. Mann, Van der Waals black hole. *Phys. Lett. B* **737**, 277 (2014)
23. J. Xu, L. Cao, Y. Hu, P-V criticality in the extended phase space of black holes in massive gravity. *Phys. Rev. D* **91**, 124033 (2015)
24. S.H. Hendi, S. Panahiyan, B.E. Panah, Extended phase space thermodynamics and P-V criticality of black holes with Born–Infeld type nonlinear electrodynamics. *Int. J. Mod. Phys. D* **25**, 1650010 (2016)
25. S. Hendi, M.H. Vahidinia, Extended phase space thermodynamics of black holes with nonlinear source. *Phys. Rev. D* **88**, 084045 (2013)
26. J. Mo, G. Li, X. Xu, Effects of power-law Maxwell field on the van der Waals like phase transition of higher dimensional dilaton black holes. *Phys. Rev. D* **93**, 084041 (2016)
27. G. Li, Effects of dark energy on P-V criticality of charged AdS black-holes. *Phys. Lett. B* **735**, 256 (2014)
28. G. Ruppeiner, Riemannian geometry in thermodynamic fluctuation theory. *Rev. Mod. Phys.* **67**, 605 (1995)
29. S.W. Hawking, *Phys. Rev. D* **13**, 191 (1976)
30. S.W. Hawking, D.N. Page, *Commun. Math. Phys.* **87**, 577 (1983)
31. S. Chaudhary, A. Jawad, M. Yasir, *Phys. Rev. D* **105**, 024032 (2022)
32. M.U. Shahzad, M.A. Nazir, A. Jawad, *Phys. Dark Univ. D* **32**, 100828 (2021)
33. Ö. Ökcü, E. Aydiner, *Eur. Phys. C* **78**, 123 (2018)
34. A. Haldar, R. Biswas, *Eur. Phys.* **123**, 40005 (2018)
35. S. Guo, J. Pu, Q.Q. Jiang, X.T. Zu, *Chin. Phys. C D* **44**, 035102 (2020)
36. A. Cisterna et al., *Phys. Lett. B* **797**, 134883 (2019)
37. S. Guo, Y. Han, G.P. Li, *Class. Quantum Gravity* **37**, 085016 (2020)
38. P.A. Cano, A. Murcia, *Class. Quantum Gravity* **38**, 075014 (2021). [arXiv:2006.15149](https://arxiv.org/abs/2006.15149) [hep-th]
39. P.A. Cano, A. Murcia, *JHEP* **10**, 125 (2020). [arXiv:2007.04331](https://arxiv.org/abs/2007.04331) [hep-th]
40. For discussions on the general properties of static and spherically symmetric metrics satisfying the  $g_{tt}g_{rr} = -1$  condition, see e.g., [106–108]
41. Pablo Bueno, Pablo A. Cano, Javier Moreno, Guido van der Velde, Regular black holes in three dimensions. *Phys. Rev. D* **104**, 021501 (2021)
42. C. Martinez, C. Teitelboim, J. Zanelli, *Phys. Rev. D* **61**, 104013 (2000). [arXiv:hep-th/9912259](https://arxiv.org/abs/hep-th/9912259)
43. D.A. Rasheed, [arXiv:hep-th/9702087](https://arxiv.org/abs/hep-th/9702087) (1997)
44. J. Mo, G. Li, X. Xu, Combined effects of  $f(r)$  gravity and conformally invariant Maxwell field on the extended phase space thermodynamics of higher-dimensional black holes. *Eur. Phys. J. C* **76**, 545 (2016)
45. R. Cai, L. Cao, R. Yang, P-V criticality in the extended phase space of Gauss–Bonnet black holes in AdS space. *J. High Energy Phys.* **09**, 005 (2013)
46. R. Cai, Y. Hu, Q. Pan, Y. Zhang, Thermodynamics of black holes in massive gravity. *Phys. Rev. D* **91**, 024032 (2015)
47. M. Azreg-Ainou, Black hole thermodynamics: no inconsistency via the inclusion of the missing P-V terms. *Phys. Rev. D* **91**, 064049 (2015)
48. J. Sadeghi, B. Pourhassan, M. Rostami, P-V criticality of logarithmic corrected dyonic charged AdS black hole. *Phys. Rev. D* **94**, 064006 (2016)
49. S.H. Hendi, M. Momennia, *Phys. Lett. B* **777**, 222 (2018)
50. S. Sorousfar, R. Saffari, N. Kamvar, *Eur. Phys. J. C* **76**, 476 (2016)
51. G. Ruppeiner, Thermodynamics: a Riemannian geometric model. *Phys. Rev. A* **20**, 1608 (1979)
52. S.H. Hendi, S. Panahiyan, B. Eslam Panah, M. Momennia, *Eur. Phys. J. C* **75**, 507 (2015)
53. H. Oshima, T. Obata, H. Hara, *J. Phys. A Math. Gen.* **32**, 6373 (1999)
54. U. Papnoi, F. Atamurotov, S.G. Ghosh, B. Ahmedov, *Phys. Rev. D* **90**, 024073 (2014). [arXiv:1407.0834](https://arxiv.org/abs/1407.0834) [gr-qc]
55. S.-W. Wei, Y.-X. Liu, *J. Cosmol. A. P.* **201**, 063 (2013). [arXiv:1311.4251](https://arxiv.org/abs/1311.4251) [gr-qc]
56. B. Eslam Panah, K. Jafarzade, S.H. Hendi, *Nucl. Phys. B* **961**, 115269 (2020). [arXiv:2004.04058](https://arxiv.org/abs/2004.04058) [hep-th]